CellPress

Molecular Cell
Article

Assessing the ceRNA Hypothesis with Quantitative Measurements of miRNA and Target Abundance

Rémy Denzler,[1,2] Vikram Agarwal,[3,4,5] Joanna Stefano,[3,4] David P. Bartel,[3,4,*] and Markus Stoffel[1,2,*]
[1]Institute of Molecular Health Sciences, ETH Zurich, Otto-Stern-Weg 7, HPL H36, 8093 Zurich, Switzerland
[2]Competence Center of Systems Physiology and Metabolic Disease, ETH Zurich, Otto-Stern-Weg 7, 8093 Zurich, Switzerland
[3]Howard Hughes Medical Institute and Whitehead Institute for Biomedical Research, Cambridge, MA 02142, USA
[4]Department of Biology, Massachusetts Institute of Technology, Cambridge, MA 02139, USA
[5]Computational and Systems Biology Program, Massachusetts Institute of Technology, Cambridge, MA 02139, USA
*Correspondence: dbartel@wi.mit.edu (D.P.B.), stoffel@biol.ethz.ch (M.S.)
http://dx.doi.org/10.1016/j.molcel.2014.03.045

SUMMARY

Recent studies have reported that competitive endogenous RNAs (ceRNAs) can act as sponges for a microRNA (miRNA) through their binding sites and that changes in ceRNA abundances from individual genes can modulate the activity of miRNAs. Consideration of this hypothesis would benefit from knowing the quantitative relationship between a miRNA and its endogenous target sites. Here, we altered intracellular target site abundance through expression of an miR-122 target in hepatocytes and livers and analyzed the effects on miR-122 target genes. Target repression was released in a threshold-like manner at high target site abundance ($\geq$1.5 × 10^5 added target sites per cell), and this threshold was insensitive to the effective levels of the miRNA. Furthermore, in response to extreme metabolic liver disease models, global target site abundance of hepatocytes did not change sufficiently to affect miRNA-mediated repression. Thus, modulation of miRNA target abundance is unlikely to cause significant effects on gene expression and metabolism through a ceRNA effect.

INTRODUCTION

MicroRNAs (miRNAs) are an abundant class of small noncoding RNAs that regulate gene expression at the levels of mRNA stability and translation (Pillai et al., 2005; Eulalio et al., 2008; Guo et al., 2010). They pair to target sites (referred to as miRNA response elements [MREs]) within mRNAs to direct the posttranscriptional downregulation of these mRNA targets. The human genome has more than 500 miRNA genes, and miRNAs from individual gene families are able to target hundreds of different messenger RNAs (Baek et al., 2008; Friedman et al., 2009). Given that more than half of all human mRNAs are estimated to be conserved miRNA targets, miRNAs are thought to have widespread effects on gene regulation (Friedman et al., 2009). Even though many miRNA knockout models show no apparent defect under normal conditions, they frequently exhibit miRNA-dependent phenotypes when specific stresses are applied (Li et al., 2009; Brenner et al., 2010). Therefore, miRNAs are proposed to be critical regulators in stress signal mediation and modulation, where inadequate miRNA levels and responses can cause or exacerbate disease (Mendell and Olson, 2012).

Highly expressed site-containing RNAs, either found naturally or delivered as research reagents, can act as "sponges" to titrate miRNAs away from other normal targets (Ebert et al., 2007; Franco-Zorrilla et al., 2007; Mukherji et al., 2011; Hansen et al., 2013; Memczak et al., 2013). Theoretical and experimental reports have claimed that crosstalk between site-containing RNAs extends far beyond a few highly expressed sponges. Analyses of high-throughput data sets indicate that the activity of a miRNA is not just dependent on its levels but also its relative target site abundance (TA), defined as the relative number of sites within the transcriptome for that miRNA (Arvey et al., 2010; Garcia et al., 2011). One hypothesis suggests that this crosstalk has a widespread regulatory function, with the act of titrating miRNAs away from their other targets somehow explaining why so many target sites have been conserved in evolution (Seitz, 2009). This idea is extended to the notion that many miRNA targets act as competitive endogenous RNAs (ceRNAs) that modulate the repression of other targets as their expression increases or decreases (Salmena et al., 2011; Tay et al., 2011). Experimental evidence for such a ceRNA crosstalk was initially described for the tumor-suppressor gene *PTEN*, which appears to be regulated by the abundance of its pseudogene (*PTENP1*) in a DICER-dependent manner (Poliseno et al., 2010). Recent studies have reported the potential physiological relevance of other ceRNAs, including a long noncoding RNA that regulates muscle differentiation (Cesana et al., 2011), an overexpressed 3′ untranslated region (3′ UTR) inducing cancer in transgenic mice (Fang et al., 2013), and a circular RNA (circRNAs) regulating miR-7 activity in the CNS (Hansen et al., 2013; Memczak et al., 2013). However, such studies have used cancer cell lines with abnormal miRNA and ceRNA expression (Poliseno et al., 2010; Karreth et al., 2011), leaving their physiological relevance in primary cells unclear.

The ceRNA hypothesis is controversial because it is difficult to imagine how the change in expression of individual miRNA targets, which each typically contribute a miniscule fraction of the TA, could possibly influence enough miRNA molecules to affect

regulation of other targets. Consideration of the ceRNA hypothesis would clearly benefit from quantitative knowledge of the intracellular relationship of miRNAs and their corresponding target sites. Although some attempts have been undertaken to evaluate this relationship, the data were typically acquired in silico (Ala et al., 2013; Figliuzzi et al., 2013), in vitro with purified components (Wee et al., 2012), or in experimental setups in which rapidly dividing cells were transfected with synthetic miRNAs, which complicate any interpretations more quantitative than relative comparisons (Arvey et al., 2010; Garcia et al., 2011; Tay et al., 2011). A more recent study not subject to these limitations reported that miRNA efficacy tended to be higher for miRNAs with lower predicted target:miRNA ratios but did not address the question of how much change in ceRNA might be required to detectably influence miRNA efficacy (Mullokandov et al., 2012).

In this study, we analyzed the stoichiometric relationship of miR-122 and its target sites by manipulating TA through controlled expression of a validated target of miR-122 in primary hepatocytes and livers. miR-122 has been linked to important human diseases, such as hepatitis C, liver cancer, and hypercholesterolemia, and its target genes have been well characterized (Jopling et al., 2005; Krützfeldt et al., 2005; Esau et al., 2006; Tsai et al., 2009). Our absolute quantification of relevant entities in primary cells and disease states provided insights on the relationship between miR-122 TA and miR-122 activity. These results will facilitate future studies predicting the biologically relevant range of TAs of other miRNAs and the magnitude of change in target abundance required to influence gene expression through a ceRNA mechanism.

RESULTS

miRNA Target Derepression Is Detected at a High Threshold of Added MREs

To assess the relationship between a miRNA and its MREs and the effect of this relationship on target gene regulation, we chose the highly expressed liver-specific miR-122 as a model system. We manipulated endogenous MREs in a controlled manner by overexpressing a full-length AldolaseA (*AldoA*) mRNA, a strong and validated target of miR-122 (Krützfeldt et al., 2005), using recombinant adenoviruses (Ad-AldoA) carrying either a mutated (Mut), one (1s), or three (3s) miR-122 binding site(s) (Figures 1A and S1A). To eliminate potential off-target effects mediated by the AldoA protein, we introduced a premature stop codon that prevented translation of AldoA protein (Figure S1B).

To assess the stoichiometric relationship of miR-122 and the added MREs in primary hepatocytes, we measured the absolute number of these entities per cell. Quantitative RT-PCR measurements calibrated with an internal standard curve of synthetic miRNA revealed that miR-122 was expressed at 1.2×10^5 molecules per cell (Figure 1B), which was comparable to levels previously reported (Bissels et al., 2009). As expected, miR-16 and miR-33 were each expressed at fewer copies per cell (1.1×10^4 and 1.2×10^3, respectively). Next, we measured the increased miR-122 target abundance after infecting hepatocytes with Ad-AldoA at three different multiplicities of infection (MOI; 2, 20, and 200) with our constructs that introduced zero, one, or three miR-122 MREs per *AldoA* transcript. Adenovirus constructs showed very high transduction efficiencies (Figure S2A), and a linear correlation was observed between viral dose and green fluorescent protein (*GFP*) mRNA, which was expressed from an independent promoter in the Ad-AldoA vector (Figure 1C). Similar results were observed when monitoring GFP protein levels (Figures S2B and S2C). At MOI 200, *AldoA* transcripts increased from 3.3×10^3 (endogenous levels) to $0.8–1.1 \times 10^6$ molecules per cell (Figure 1D), introducing up to 2.6×10^6 *AldoA* MREs per cell (Figure 1E). The ratio of *AldoA* to *GFP* mRNA showed that the *AldoA* transcripts were repressed in an MRE-dependent manner at MOI 2 and 20, which confirmed that miR-122 was functionally engaging the MREs within these transcripts (Figure 1F). This regulation disappeared at MOI 200, suggesting that, at this very high MOI, *AldoA* transcript overwhelmed the regulatory capacity of miR-122 (Figure 1F). Quantification of miR-122 confirmed that the loss of regulation was not due to a loss in miR-122; even at very high levels, Ad-AldoA did not influence the levels of either miR-122 or two control miRNAs, although it did reduce miR-33 by 2-fold (Figure 1G).

Having observed a loss in *AldoA* repression at a high MOI, we reasoned that high levels of *AldoA* transcript could act as a sponge to also derepress cellular miR-122 targets. Indeed, known miR-122 targets, but not a control transcript *ApoM*, increased at a high MOI (Figures 1H and S2D). Interestingly, this derepression was confidently detected only when *AldoA* MREs exceeded $1.5–2.7 \times 10^5$ per cell. This threshold corresponded to 1.25–2.25 MREs per miR-122 molecule. Once this threshold was exceeded, additional *AldoA* MREs led to greater miR-122 target derepression, and the magnitude correlated with the number of miR-122 sites introduced by *AldoA* transcripts. Altogether, these data demonstrate that derepression mediated through increased expression of a miR-122 target can occur but can be detected only after exceeding a high threshold of added MREs.

The High Threshold Persists after Lowering miR-122 Activity

Two scenarios might explain the high threshold of added MREs required to observe endogenous target derepression. The "excess miRNA" scenario posits that very abundant miRNAs are present in excess over their targets, and thus competing MREs would need to titrate this excess binding capacity before they could exert an observable effect on endogenous target repression. Our case of miR-122 in hepatocytes would be one of the more attractive candidates for this scenario, given that miR-122 is the most abundant miRNA in hepatocytes (Landgraf et al., 2007). Indeed, its abundance of 1.2×10^5 molecules per cell is among the highest reported for a miRNA in any mammalian system. The second scenario is the "high TA" scenario. In this scenario, the effective number of miRNA binding sites within cellular transcripts is so high that even highly expressed miRNAs are mostly bound to a site at any moment in time, and thus the number of competing MREs would need to approach this high effective number of sites before the competing MREs could exert an observable impact on endogenous target repression. The idea of many miRNA binding sites within cellular transcripts is supported by reports that many miRNAs have hundreds of

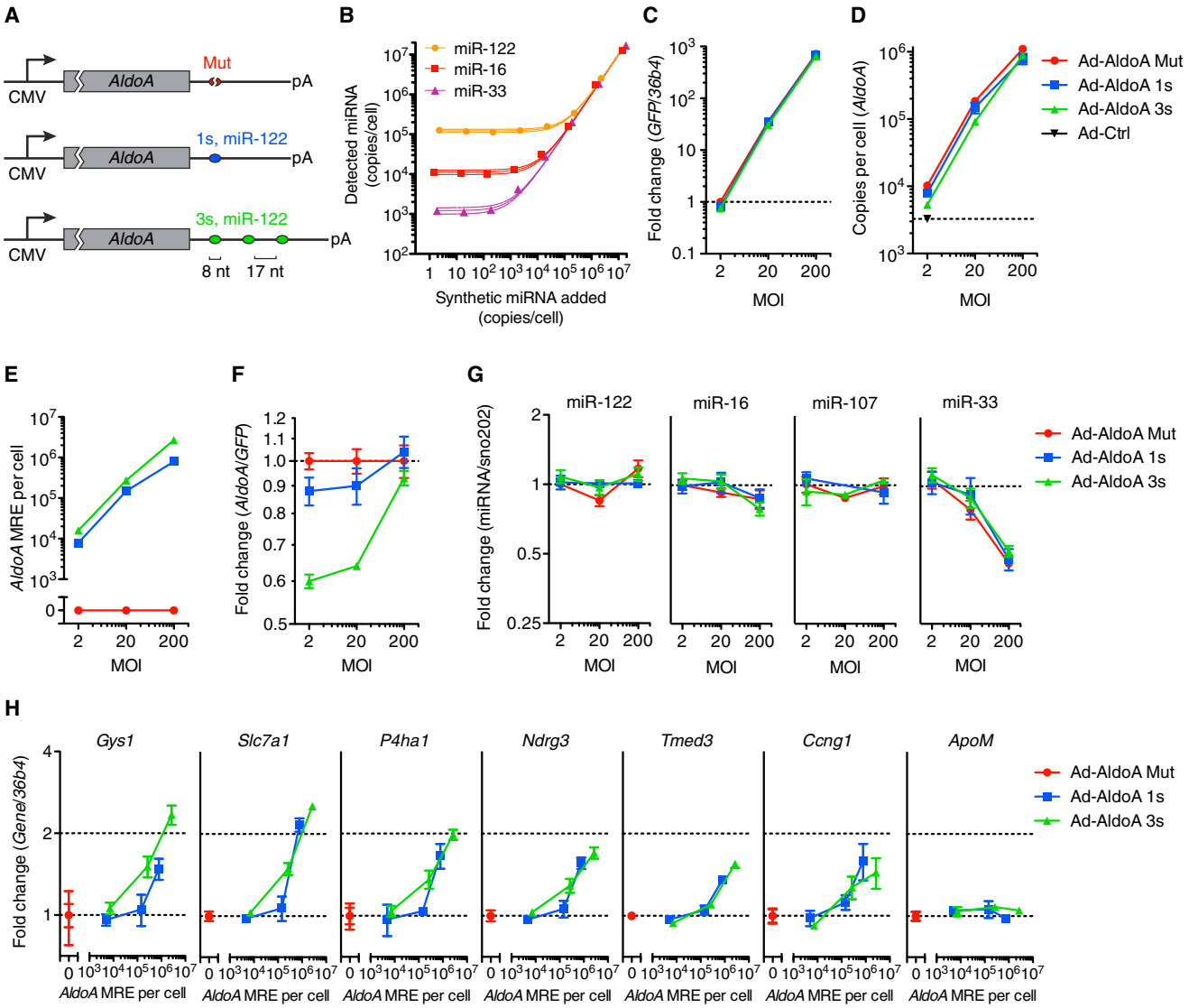

Figure 1. miRNA Target Derepression Is Detected at a High Threshold of Added MREs

(A) Schematic overview of the different *AldoA*-expressing adenovirus constructs (Ad-AldoA) harboring either one (1s, blue) or three (3s, green) miR-122 binding sites or a mutated site (Mut, red). Ad-AldoA 3s contained three 8 nt seed matches of miR-122 separated by 17 nt spacers. See also Figure S1.

(B) Absolute miRNA quantification of primary hepatocyte cell lysates spiked with different amounts of synthetic miRNA. Solid lines represent linear regression data with respective 95% confidence intervals.

(C–H) Primary hepatocytes infected with different multiplicities of infection (MOI) of the Ad-AldoA constructs. Relative gene expression of *GFP* (C) and *AldoA* (F) and absolute copy numbers per cell of *AldoA* (D) and *AldoA* MRE (E). Relative expression of miRNAs (G) or miR-122 target genes and a control nontarget gene (*ApoM*) (H). See also Figure S2.

GFP and miRNA expression are relative to Ad-AldoA Mut at MOI 2; *AldoA*, miR-122 target genes and the control gene are relative to the respective Ad-AldoA Mut at given MOI. Data represent mean ± SEM (n = 3) for all panels.

conserved MREs (Friedman et al., 2009), miRNAs also repress many additional mRNAs with nonconserved MREs (Farh et al., 2005; Krützfeldt et al., 2005; Giraldez et al., 2006; Baek et al., 2008), and high-throughput crosslinking identifies many additional binding sites that would not be classified as MREs because they don't mediate detectable repression (including many sites within open reading frames and marginally effective sites elsewhere) but would nonetheless add to the effective number of binding sites (Hafner et al., 2010). These two scenarios predict two very different responses to miRNA reduction. In the excess miRNA scenario, miRNA reduction would lower the excess miRNA capacity and thereby lower the threshold of added MREs required to observe endogenous target derepression. In the high TA scenario, the effective number of sites already exceeds the miRNA abundance, and, more importantly, the threshold relates to the effective number of binding sites and

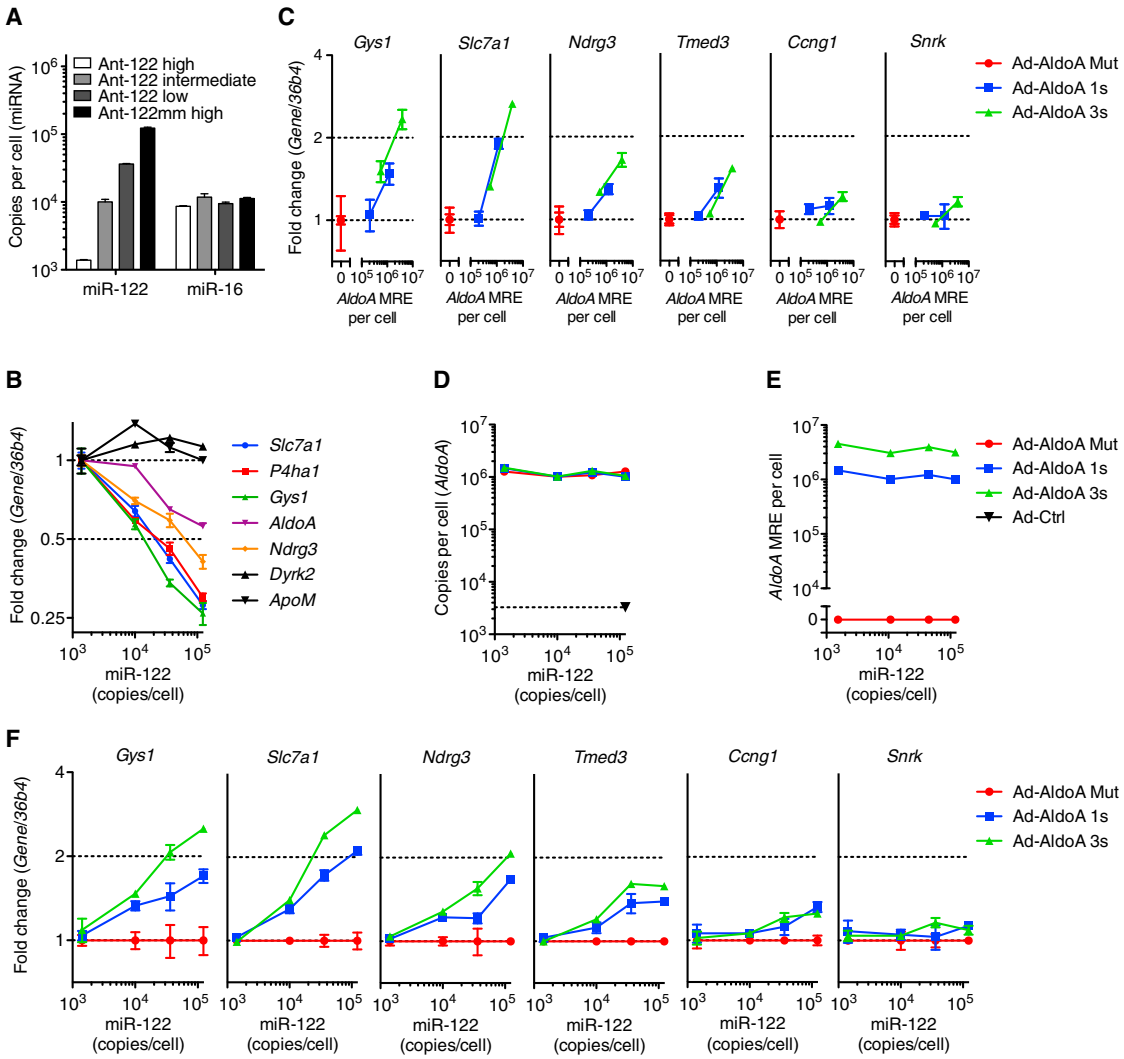

Figure 2. The High Threshold Persists after Lowering miR-122 Activity

(A) Absolute miRNA copy numbers per cell or (B) relative expression of miR-122 target genes and control nontarget genes (*Dyrk2* and *ApoM*) in primary hepatocytes from mice treated with Ant-122mm or different concentrations of Ant-122. Values for miR-122 target and control genes are normalized to that of the lowest miR-122 concentration.

(C) Relative expression of miR-122 target genes and a nontarget gene (*Snrk*) in primary hepatocytes with 3-fold decreased miR-122 levels shown in (A), infected with MOI 20 and 200 of Ad-AldoA Mut (red), 1s (blue), or 3s (green).

(D–F) Primary hepatocytes shown in (A) infected with MOI 200 of the three Ad-AldoA constructs. Absolute copy numbers per cell of *AldoA* (D) and *AldoA* MRE (E) in relation to miR-122 copy numbers.

(F) Relative expression of miR-122 target genes and control nontarget gene (*Snrk*) normalized to Ad-AldoA Mut of the respective miR-122 condition.

Absolute miRNA copy numbers were calculated by multiplying relative abundance (miRNA/snoRNA202) that were normalized to Ant-122mm with the copy number evaluated in Figure 1B. Data represent mean ± SEM (n = 4) for all panels.

not the number of miRNA molecules. Thus, in this scenario, miRNA reduction would lower the degree to which targets are repressed, but it would not lower the threshold of added MREs required to observe derepression.

By analyzing whether a change in miRNA levels influences the threshold for the number of added *AldoA* MREs needed for derepression, we sought to experimentally evaluate which scenario applies. We injected three different amounts (low, intermediate, and high) of Antagomir-122 (Ant-122) into mice and found that miR-122 levels detected in the primary hepatocytes were reduced to 0.3, 0.08, and 0.01 of that observed in hepatocytes from mice injected with the mismatch Ant-122 control (Ant-122mm; Figure 2A) (Krützfeldt et al., 2005). Target gene derepression correlated with decreased miR-122 levels, which confirmed that our miR-122 quantification reflected miR-122 activity (Figure 2B). Next, we studied the effect of controlled overexpression of *AldoA* MRE on target gene derepression in hepatocytes with a modest 3-fold decrease in miR-122 levels. Interestingly, derepression was detected only when exceeding the threshold of 2 × 10^5 *AldoA* MREs per cell (Figure 2C). This

threshold was comparable to that observed in cells without reduced miR-122 levels, which indicated that the reason for the threshold was not excess miR-122 binding capacity. Instead, high TA is the more likely reason that the amount of added MREs must exceed a very high level before exerting an observable effect.

Some studies claiming ceRNA-mediated gene regulation focus on the number of sites to miRNA families that are shared between the ceRNAs without differentiating between those miRNAs that are expressed at a level sufficient to repress target genes and those that are not (Jeyapalan et al., 2011; Fang et al., 2013). To demonstrate that derepression can only occur in conditions in which target gene repression is happening, we infected hepatocytes harboring different miR-122 levels with Ad-AldoA at MOI 200 and measured target derepression. Levels of *AldoA* and respective *AldoA* MRE copy number per cell were comparable in all Ant-treated samples (Figures 2D and 2E). miR-122 target gene derepression was between 1.5- and 2.5-fold in hepatocytes with high miR-122 levels and below 1.5-fold in cells with intermediate miR-122 activity (Figure 2F). No target gene derepression was observed in hepatocytes with the lowest miR-122 levels. Altogether, these data demonstrate that miRNAs need to exceed an expression level sufficient to repress their targets in order for targets to be derepressed in a ceRNA-dependent manner.

The Magnitude of Derepression Correlates with Predicted Site Efficacy and Number of Added *AldoA* MREs

Previous ceRNA studies have focused on only one or a few targets of a miRNA even though a ceRNA change that influences miRNA activity would be expected to affect more than a few targets. Because any perturbation of a cell might result in spurious expression changes in a few predicted targets, a transcriptome-wide analysis examining the preferential effect on predicted targets would more confidently detect the influence of a competing RNA. Therefore, we extended our quantitative analysis to the transcriptome and performed RNA sequencing (RNA-seq) on primary hepatocytes infected with different Ad-AldoA constructs at MOI 2, 20, and 200. Then, we analyzed the relationship between the derepression of predicted targets and their site number, site type (6, 7, and 8 nt sites), site position, and other determinants used by TargetScan to calculate total context+ scores of predicted miRNA targets (Lewis et al., 2005; Grimson et al., 2007; Garcia et al., 2011). When predicted targets of miR-122, miR-33, miR-16, or abundant miRNA families in liver (either let-7, miR-192, or a combination of the next four most abundant families) were distributed into ten context+ score bins and plotted against their median fold change, the effect of target derepression was evident for predicted targets of miR-122 but not for those of any of the other miRNA families (Figures 3A, S3A, S3B, and Table S1). As expected, the extent of target derepression correlated with the magnitude of the context+ score as well as with the number of added *AldoA* MREs. These correlations were also observed in the fold change distributions of miR-122 predicted targets (Figure 3B), and analogous results were obtained when stratifying predicted targets by site type (Figure S3C). Regardless of how we grouped the predicted targets, the same threshold of $\geq 1.5 \times 10^5$ added MREs per cell was required in order to observe miR-122 derepression. We also studied target gene derepression in primary hepatocytes treated with Ant-122 or the mismatch control Ant-122mm and found that the strongest predicted targets (e.g., those with a context+ scores below –0.2) were significantly derepressed in the Ant-122-treated conditions (Figures S3D–S3G and Table S1).

Modest Changes in Target Abundance Are Induced by Metabolic Stress and Disease

Next, we sought to investigate the quantitative relationship between MREs added upon Ad-AldoA infection and those normally contributed by mRNAs of primary hepatocytes. First, we tested how transcript abundances, measured by RNA-seq in fragments per kilobase of transcript per million fragments mapped (FPKM) correlated with the absolute copy numbers determined by quantitative PCR. To this end, we compared the expression levels of four genes that are differentially expressed in primary hepatocyte and liver samples and found a linear relationship between FPKM and absolute copy numbers over several orders of magnitude (Figure 4A), which allowed us to transform RNA-seq data to absolute mRNA copies per cell. Then, we compared how *AldoA* transcript abundance corresponded to genome mRNA abundance at different MOIs of Ad-AldoA-infected hepatocytes. The *AldoA* contribution ranged from 0.3%–0.8% at MOI of 2, 6%–12% at MOI 20, and > 50% of all mRNA at MOI 200 (Figure 4B). In contrast, the largest endogenous contributor to the transcriptome of primary hepatocytes was Transferrin (*Trf*), which made up only 1.6% of the mRNA (30,000 molecules per cell). Thus, the level of *AldoA* at the MOI for which derepression was observed (MOI 20 and 200), was substantially higher than that of transcripts from any single cellular gene.

We also attempted to place the *AldoA* abundance within the context of the miR-122 TA within the hepatocyte transcriptome. A previous estimate of miRNA TA considers all of the 7 and 8 nt sites for that miRNA within expressed 3′ UTRs (Garcia et al., 2011). This TA might over- or underestimate the effective number of binding sites of the transcriptome, depending on the extent to which some of these sites are inaccessible (e.g., because they are occluded by mRNA secondary structure or RNA binding proteins) and the extent to which intracellular binding capacity is augmented by additional sites (e.g., 6 nt sites, other marginal sites, and nonconventional sites as well as sites in ORFs, 5′ UTRs, or noncoding RNAs), many of which might add to the effective number of binding sites without mediating repression. Despite these uncertainties, relative TA estimates for different miRNAs provide a useful basis for distinguishing the more effective miRNAs from the less effective ones (Garcia et al., 2011).

Our conclusion that competing MREs begin to exert their effects as they approach the miRNA binding capacity of the transcriptome provided the means to evaluate the relationship between the previous TA estimate and the apparent number of binding sites. When calculated as before (summing 7 and 8 nt sites in transcriptome 3′ UTRs), the miR-122 TA in hepatocytes at Ad-AldoA MOI 2 was 1.8×10^5 sites per cell, which essentially matched the threshold of added MREs required to begin to observe derepression. The addition of 6 nt sites in the analysis increased the number to 4.4×10^5 miR-122 sites per cell. Given that this was still below the number of added MREs required to

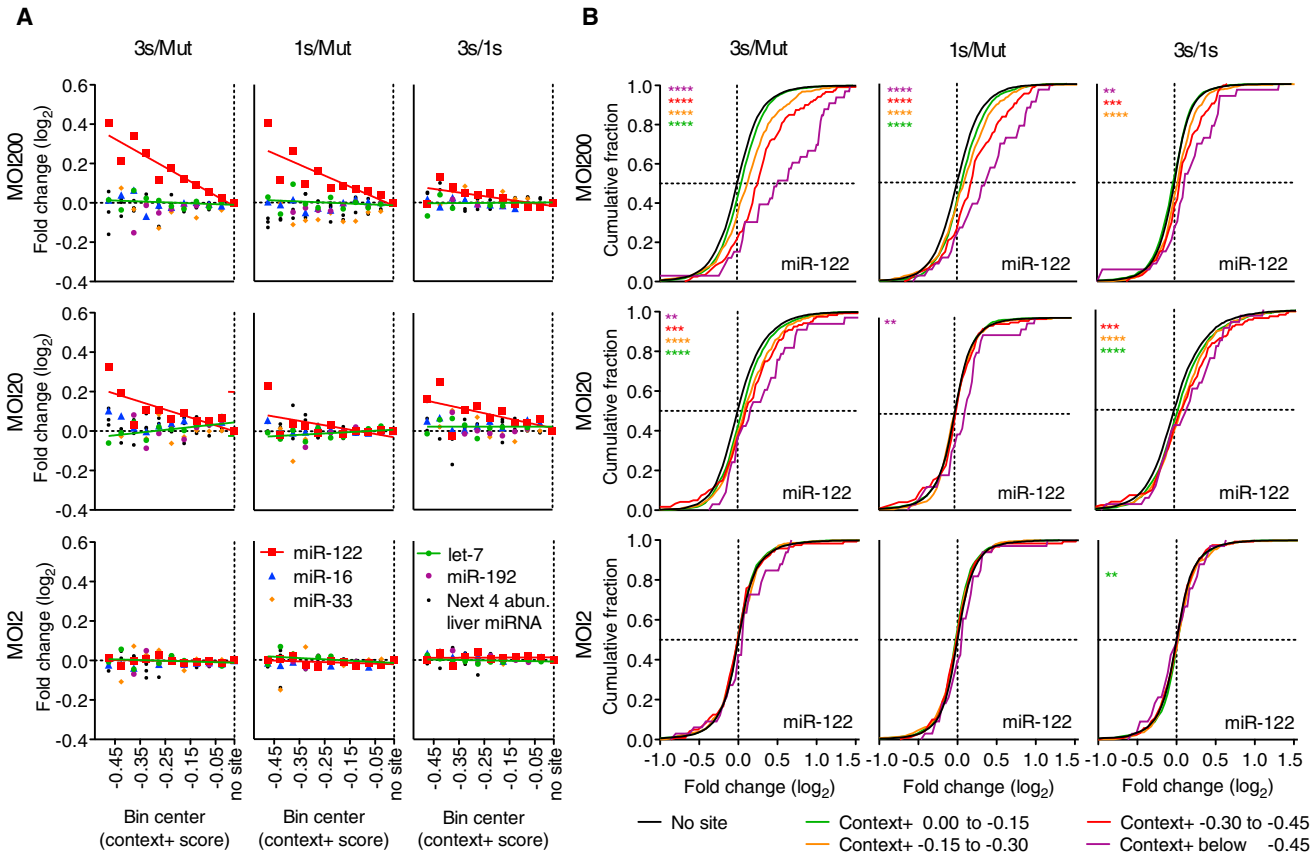

Figure 3. The Magnitude of Derepression Correlates with Predicted Site Efficacy and Number of Added *AldoA* MREs

(A and B) RNA-seq results showing derepression of predicted targets from primary hepatocytes infected with MOI 200, 20, and 2 of Ad-AldoA Mut, 1s, or 3s shown in Figures 1C–1H.

(A) Predicted targets of miR-122 (red), miR-16 (blue), miR-33 (orange), let-7 (green), miR-192 (purple), or a combination of the next four most abundant liver miRNA families (black) were grouped into ten bins based on their context+ scores. For each miRNA family, the median $\log_2$ fold change is plotted for the predicted targets in each bin. Medians were normalized to that of the bin with genes without sites. Bins each had at least ten genes; see Figure S3B for group sizes.

(B) Cumulative distributions of mRNA changes for genes with no miR-122 site (black) or predicted target genes with the indicated context+ score bins (color). Number of genes per bin: black, 6,629; green, 1,693; orange, 434; red, 120; purple, 33. *p < 0.05, **p < 0.01, ***p < 0.001, ****p < 0.0001, one-sided Kolmogorov-Smirnov (K-S) test.

See also Figure S3 and Table S1.

observe half-maximal derepression, for all additional analyses, we considered this revised TA estimate (all 6, 7, and 8 nt sites within the transcriptome 3′ UTRs), which we define as the apparent TA (or TA_{app}), as a conservative estimate of the effective number of miRNA sites.

Next, we calculated how *AldoA* MREs influenced the miR-122 TA_{app} (Figure 4C) and what fraction of the TA_{app} *AldoA* MREs contributed (Figure 4D). Because only very highly expressed genes could reach the levels required to affect TA, we searched for endogenous transcripts that quantitatively contributed the largest percentage to transcriptome TA_{app}. *Actinb* (*Actb*), which contributed 5.5% of the TA_{app}, was the largest potential contributor to miR-122 site abundance in primary hepatocytes (Figure 4E), although this contribution was less than the 30% contribution required for *AldoA* to detectably modulate miR-122 repression (Figure 4D). When using the same approach to estimate TA_{app} for let-7, miR-16, miR-33, miR-192, or each of the next four most abundant miRNA families, the transcript with the largest contribution to any TA_{app} was Albumin (*Alb*), which contributed ~3% of the miR-103 TA_{app} (Figure 4E).

As a major metabolic integrator of physiological processes, the liver exhibits profound changes of gene regulation in response to insulin signaling and cholesterol metabolism. To examine whether these changes might affect miRNA TA_{app}, we analyzed two models with severe pathological changes in cholesterol metabolism (LDLR-deficient mice, *Ldlr*$^{-/-}$) (Ishibashi et al., 1993) and hepatic steatosis (high-fat diet [HFD] mice; Figures 4F, S4A, and Table S2) (Channon and Wilkinson, 1936). We also examined livers that were perfused in the absence and presence of insulin, representing fasted and fed states, respectively (Figure S4B and Table S2). In all livers studied, *Alb* and Transthyretin (*Ttr*) contributed ~10%–20% to TA_{app}. The only strong contributor that was differentially regulated in any model was major urinary protein 7 (*Mup7*), which essentially disappeared

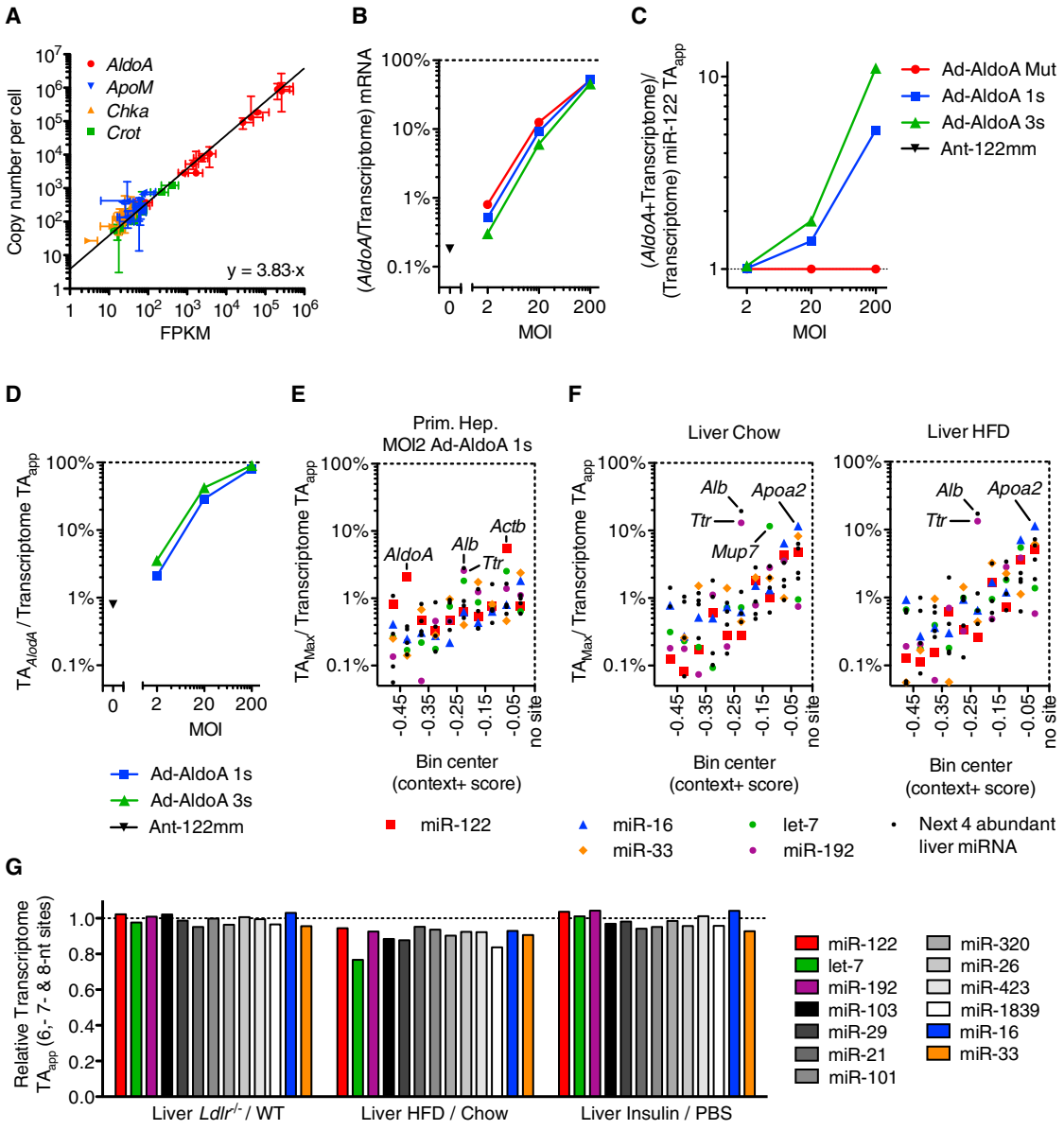

Figure 4. Modest Changes in Target Abundance Are Induced by Metabolic Stress and Disease

(A) Relationship between FPKM from RNA-seq data and absolute quantification with qPCR. Represented are four genes quantified in all 11 primary hepatocyte samples plus wild-type and *Ldlr*$^{-/-}$ liver samples. Line represents linear regression of data points. Data represent mean ± 95% confidence intervals.

(B–D) RNA-seq data from primary hepatocytes infected with MOI 200, 20, and 2 of Ad-AldoA Mut, 1s, or 3s shown in Figure 1C–H. Data represent mean ± SEM (B). Contribution of *AldoA* mRNA to the sum of genome mRNA. Increase of transcriptome miR-122 TA_{app} (C) and the respective contribution of *AldoA* MRE (D) to total transcriptome miR-122 TA_{app} mediated by the different Ad-AldoA constructs and viral concentrations.

(E and F) Fractional contribution of the largest potential contributors to transcriptome TA_{app} in primary hepatocytes infected with MOI 2 of Ad-AldoA 1s (E) or in wild-type livers (F) originated from mice either fed normal chow or high-fat diet (HFD). Potential contributors were binned by their context+ scores, and the top potential contributors are plotted within each bin. See also Figure S4 and Table S2.

(G) Relative target abundance of livers from models of physiological (insulin) or disease/stress states (*Ldlr*$^{-/-}$ and HFD).

in livers of HFD mice, causing its contribution to TA_{app} to decrease from 11.6% in normal livers to 0.01% in HFD livers. *Alb*, the most highly expressed mRNA and the largest potential contributor of sites for the miR-103 family, had the potential to reduce TA_{app} by a maximum of only 20% when fully silenced. Conversely, a 30% increase in target abundance would require the most abundant liver transcript to increase ~2.5-fold.

Because none of the small number of genes that alone could alter TA_{app} in a consequential way appeared to do so, we tested whether a substantial change could be achieved through collective changes of all mRNAs. Evaluation of TA_{app} changes for

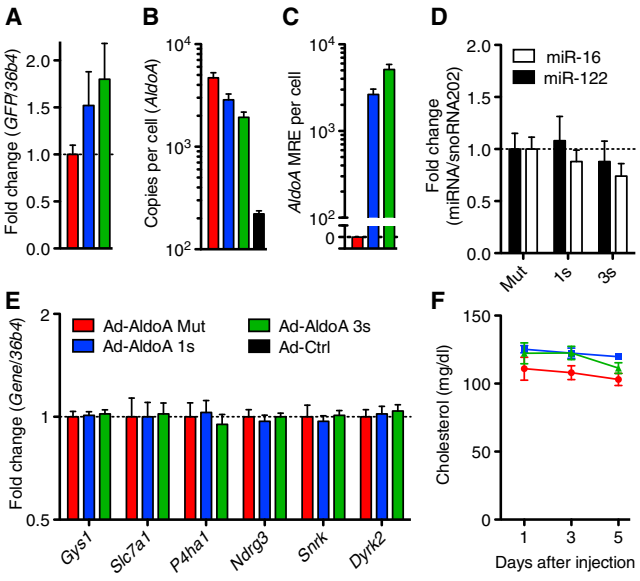

Figure 5. No ceRNA Effect Is Detected In Vivo

(A–E) Mice were injected with Ad-AldoA Mut (red, n = 6), 1s (blue, n = 6), or 3s (green, n = 5), and gene expression analysis was performed 5 days post-infection. Relative gene expression of *GFP* (A), absolute copy numbers per cell of *AldoA* (B), and added *AldoA* MREs (C). Relative expression of miRNAs (D) and miR-122 target genes or control nontarget genes (*Snrk* and *Dyrk2)* (E). (F) Plasma cholesterol levels of Ad-AldoA-treated mice at days 1, 3, and 5. The Ad-AldoA used in this experiment expressed the full-length protein. Data represent mean ± SEM.

miR-122, the next ten most abundant miRNA families in liver, miR-33, and miR-16 revealed that TA_{app} values for these miRNAs were not altered more than 25% in any physiological or disease model, and most changes were below 10% (Figure 4G). We also calculated TA_{app} values for the liver samples and primary hepatocytes infected with Ad-AldoA at MOI 20, in which derepression was observed. Transcriptome TA_{app} values ranged between 2.5–7.5 × 10^5 sites per cell in liver models, and between 3.6–13 × 10^5 in primary hepatocytes (Figure S4C).

No ceRNA Effect Is Detected In Vivo

To examine the influence of *AldoA* MREs on target gene derepression and relevant physiological endpoints in vivo, we injected wild-type mice with 3 × 10^9 plaque-forming units of Ad-AldoA and examined livers 5 days postinfection. Virally expressed *GFP*, and therefore adenovirus expression, was comparable in all conditions (Figure 5A). Ad-AldoA increased *AldoA* transcripts from 2.2 × 10^2 (endogenous levels) to 4.7 × 10^3 copies per cell (Figure 5B), introducing between 2.6 × 10^3 and 5.1 × 10^3 miR-122 MREs per cell with Ad-AldoA 1s or 3s, respectively (Figure 5C). Overexpression of the Ad-AldoA constructs did not change levels of miR-122 or a control miRNA (Figure 5D). No derepression of any miR-122 target or control gene (*Snrk* and *Dyrk2*) was observed (Figure 5E). Furthermore, we did not detect changes in serum cholesterol levels (Figure 5F), which decrease upon miR-122 inhibition by Ant-122 (Krützfeldt et al., 2005). As predicted from our studies of primary hepatocytes, these results showed that introduction of 5.1 × 10^3 miR-122 MREs per cell was insufficient to induce either target derepression or downstream physiological responses.

DISCUSSION

Our results support a model in which the changes in ceRNAs must begin to approach the TA of miRNA before they can exert a consequential effect on the repression of targets for that miRNA. For miR-122 in hepatocytes, derepression began to be observed at a threshold of 1.5 × 10^5 added sites per cell, a value exceeding the physiological levels of any endogenous target as well as the aggregate change of all predicted targets in different disease states. Altogether, our data imply that a ceRNA effect mediated through a single miRNA family in a physiological or disease setting of the liver is unlikely. However, we cannot exclude the possibility that unidentified highly abundant and regulated noncoding RNAs (including circRNAs) might substantially contribute to the pool of transcriptome binding sites.

In stating that changes in endogenous targets are unlikely to mediate a ceRNA effect that is detectable, we do not mean to imply that there is absolutely no molecular consequence of changing the level of an endogenous target. Large changes in each of several dozen target genes could alter TA by 1% or sometimes more, which would influence the repression of other targets but not to an extent that would be detectable by our methods. For example, an increase in TA by 5% is expected to decrease repression of other targets by approximately 5%, causing a target that was previously repress by 30% to now be repressed by approximately 28.5%—a change too small to be detected and presumably too small to be of biological consequence.

Studying the stoichiometric relationship of an miRNA and its TA and assessing the effect of this relationship on target gene regulation has been challenging. Estimates of TA have proven to be particularly difficult, given that the extent to which ineffective or marginally effective binding sites contribute to TA has been unclear, and no experimentally determined TA values had been obtained. Our experiments indicate that the TA_{app} for miR-122 in the hepatocyte transcriptome is 4.4 × 10^5 sites per cell. Although this estimate corresponds to the number of ≥6 nt seed-matched sites for miR-122 in the 3′ UTRs, we do not presume that all UTR sites mediate repression. Indeed, the TA_{app} is expected to exceed the number of miR-122 MREs, given that sites that bind the miRNA too transiently to exert repression (including most sites in ORFs) would nonetheless contribute to TA_{app}.

We qualify our TA estimate as an "apparent TA" for two reasons: first, our miR-122 TA_{app} is expected to be a function of the strength of the miR-122 site that was used in its determination. The *AldoA* site is relatively strong (context+ score of −0.4; Figure 4E). Had we empirically estimated the TA with a weaker miR-122 site, more of the added sites would have been required to approach half derepression, and thus the TA_{app} value would have been correspondingly higher. Second, the endogenous sites contribute to TA_{app} in proportion to their ability to sequester the miRNA, and thus because many weak sites (ranging from those typically classified as nonspecific sites to those that might be more specific yet nonetheless ineffective or marginally

effective) each make partial contributions to the TA_{app}, the actual number of sites that contributed is expected to greatly exceed the TA_{app}. When considering this second point, estimating a TA_{app} is of greater practical value than knowing the total number of endogenous sites that helped sequester the miRNA.

Our miR-122 TA_{app} was empirically derived on the premise that using Ad-AldoA to double the effective miR-122 TA and thereby decrease the number of encounters between miR-122 and its endogenous targets by half would lead to a corresponding decrease in endogenous target repression. If the amount of miR-122-mediated repression is not a simple linear function of the number of encounters with its targets, then TA_{app} would need to be corrected accordingly. For other miRNAs, TA_{app} values were estimated starting with the miR-122 TA_{app} and assuming that relative values for different miRNAs would scale in proportion to their numbers of UTR sites—an assumption supported by studies showing that miRNA efficacy negatively correlates with the relative numbers of UTR sites (Arvey et al., 2010; Garcia et al., 2011; Mullokandov et al., 2012). Despite any uncertainty arising from these simplifying assumptions, our TA_{app} estimates have the unique benefit of being founded on intracellular experimental observations.

This experimental grounding produced TA_{app} values much higher than those previously assumed. For example, previous modeling of the quantitative relationships between miRNAs and their targets assumed that a typical miRNA had ~500 target sites per cell (Wee et al., 2012). Modeling based on this low number of targets suggests that for moderately expressed miRNAs, adding only 500 sites through increased ceRNA expression could double the expression of a repressed mRNA, whereas for more highly expressed miRNAs, many more sites would be required to exert an effect (Mullokandov et al., 2012; Wee et al., 2012). Our results in hepatocytes indicate that TA_{app} values for the eleven most abundant miRNA families ranged from 2.5×10^5 to 7.5×10^5 sites, about 1,000 times greater than the value previously assumed. This substantially revised estimate of effective TA leads to a different and somewhat simplified picture of the potential for regulation through ceRNAs. In our model, miRNA levels matter only in so much as the miRNA must reach a level sufficient to repress a target mRNA. For any miRNA exceeding this level, the potential for ceRNAs to influence repression is simply a matter of whether the ceRNAs add or subtract enough sites to meaningfully influence the TA_{app}. Because TA_{app} is a function of the number of seed-matched sites in the transcriptome and substantially exceeds the level of even the most highly expressed miRNA, the ceRNA difference required to achieve half-maximal effects is independent of the miRNA level. Thus, our insights and results indicate that repression by even moderately expressed miRNAs would be difficult to detectably change through a ceRNA effect.

Under extreme physiological and disease conditions, target abundances were not changed more than 10% for most miRNA families. The maximum change of ~25% was observed for the let-7 miRNA family in mice fed an HFD versus a chow diet. Interestingly, in this condition, a single highly expressed gene (*Mup7*) accounted for ~50% of the total decrease in let-7 target abundance. A recent phase I trial for RNAi therapy of Ttr amyloidosis reduced human TTR levels by >80% (Coelho et al., 2013). Such a strong reduction of the *TTR* transcript, which contributes ~10% of the miR-192 TA_{app} in mouse livers, would account for a decrease in miR-192 target abundance analogous to that observed for *Mup7* and let-7 in the HFD versus chow diet, a change not expected to detectably affect miRNA activity.

The conclusion that only large contributors to TA_{app} can detectably influence the miRNA activity agrees with our in vivo experiments; in normal liver, *AldoA* is expressed at $\sim 2.4 \times 10^2$ copies per cell and is among the thousand most highly expressed genes. Still, a 9-fold increase in transcript levels after Ad-AldoA 3s infection, which added $\sim 5 \times 10^3$ MREs, increased miR-122 TA_{app} by only 2% and therefore imparted no detectable influence on target gene expression. *Mup7* and *Ttr* are among the thirty genes expressed in liver at copy numbers above 10^4 copies per cell, and therefore approaching within an order of magnitude the estimated miRNA TA_{app} values. Hence, only these 30 genes have potential on their own to perceptibly influence a TA_{app}.

Our study focused on miR-122, an unusually highly expressed miRNA. Nonetheless, the same high threshold for detectable target derepression was observed when miR-122 activity was reduced, which indicated that our conclusions apply also to more moderately expressed miRNAs. A study reporting loss of miR-20 repression when adding high levels of target mRNA also observed a threshold at high target expression (Mukherji et al., 2011). As expected, their threshold disappeared when a miR-20 sponge was used to lower miRNA activity below detection. More interestingly, they found that transfecting an miR-20 mimic increased the threshold for derepression. A possible reason that they observed a change in threshold with a change in miRNA, whereas we did not, is that their miR-20 mimic might have added enough miRNA to exceed the miR-20 TA_{app} of their cells. Another difference between their experiments and ours is that their target contained bulged sites of a type that can induce miRNA degradation (Ameres et al., 2010), which might produce an apparent shift in the threshold.

Gene expression in the liver is profoundly regulated by circadian and hormonal and nutritional states. Using livers of mice exposed to insulin signaling and to pathological conditions of cholesterol metabolism, we did not observe large changes in target abundance, raising the possibility that our findings can be generalized to other organs and disease states. Nonetheless, during cell differentiation and in the context of malignant transformation, expression of coding and noncoding RNA can change dramatically (Rhodes and Chinnaiyan, 2005; Lujambio and Lowe, 2012). In such biological settings conditions might arise in which TA_{app} is lower than in physiological settings and/or a single mRNA substantially contributes to target abundance. In principle, such alterations could make the system more amenable to ceRNA-mediated gene regulation.

EXPERIMENTAL PROCEDURES

Animal Experiments

Animals were maintained on a 12 hr light/12 hr dark cycle under a controlled environment in a pathogen-free facility at the Institute for Molecular Systems Biology, ETH Zürich. Mice were administered adenovirus through a single

tail-vein injection of 3 × 10^9 plaque-forming units in a final volume of 0.2 ml diluted in PBS and killed 5 days postinjection. Antagomir was administered through tail-vein injections on three consecutive days, and primary hepatocytes were isolated on day four. For high, intermediate, and low miR-122 inhibition, mice received 3 × 80, 40, and 20 mg/kg Ant-122, respectively. Ant-122mm (control) was used at the highest concentration. All animal experiments were approved by the ethics committee of the Kantonale Veterinäramt Zürich.

Primary Hepatocytes Isolation and Viral Infections

Primary hepatocytes of 8- to 12-week-old male C57BL/6N mice were isolated on the basis of the method described by Zhang et al. (2012). Hepatocytes were counted and plated at 300,000 cells per well in Dulbecco's modified Eagle's medium low-glucose media and adenoviruses were added in Hepatozyme media 4–6 hr after plating and harvested 24 hr postinfection. All cells were incubated at 37°C in a humidified atmosphere containing 5% CO_2.

Adenoviruses

Recombinant adenoviruses were generated as described in the Supplemental Experimental Procedures. All adenoviruses expressed *GFP* from an independent promoter. Ad-Ctrl was based on the same vector backbone (including GFP) but lacked the *AldoA* transgene.

Gene Expression Analysis

2 ug of total RNA was treated with the DNA-*free* Kit (Life Technologies) and reverse transcribed with the High Capacity cDNA Reverse Transcription Kit (Life Technologies). Quantitative PCR reactions were performed with the LightCycler 480 (Roche) employing KAPA SYBR FAST qPCR Master Mix (2×) for LightCycler 480 (Kapa Biosystems) and gene-specific primer pairs (Table S3). Relative gene expression was calculated with the ddCT method and mouse *36b4* (*Rplp0*) for normalization.

miRNA Expression Analysis

150 ng of total RNA was reverse-transcribed with the TaqMan MicroRNA Assays and Reverse Transcription Kits (Life Technologies). Quantitative PCR reactions were performed with the LightCycler 480 employing TaqMan Universal PCR Master Mix, No AmpErase UNG (Life Technologies), and TaqMan MicroRNA Assays (Life Technologies). Relative miRNA expression was calculated with the ddCT method and mouse snoRNA202 for normalization.

RNA-Seq

For single-end library construction, total RNA was depleted of rRNA with the Ribo-Zero rRNA Removal Kit (Epicenter). RNA libraries were prepared with the dUTP-based, Illumina-compatible NEXTflex Directional RNA-Seq Kit (Bioo Scientific). For paired-end library construction (performed by BGI), total RNA was enriched for poly(A) mRNA with oligo(dT) beads and treated with buffer in order to yield 200–700 nt fragments. First-strand cDNA was synthesized with random hexamer primers, and second-strand cDNA was synthesized with buffer, dNTPs, RNase H, and DNA polymerase I. cDNA was run on an Agarose gel for suitable fragment size selection followed by a purification, adaptor ligation, and PCR amplification. All libraries (both single- and paired-end) were sequenced with an Illumina HiSeq 2000 sequencing machine.

ACCESSION NUMBERS

The NCBI Gene Expression Omnibus accession number for the data reported in this paper is GSE52801.

SUPPLEMENTAL INFORMATION

Supplemental Information contains Supplemental Experimental Procedures, four figures, and three tables and can be found with this article online at http://dx.doi.org/10.1016/j.molcel.2014.03.045.

ACKNOWLEDGMENTS

We would like to thank M. Ravichandran and W. Johnston for technical assistance as well as D. Koppstein, V. Auyeung, M. Latreille, and members of the D.P.B. and M.S. labs for critically reviewing this manuscript. This material is based upon work supported under a National Science Foundation Graduate Research Fellowship (to V.A.), an ERC grant (Metabolomirs) and the NCCR (RNA and Biology; to M.S.), and NIH grant GM067031 (to D.P.B.). D.P.B. is a Howard Hughes Medical Institute Investigator. D.P.B. and M.S. are members of the scientific advisory boards of Alnylam Pharmaceuticals and Regulus Therapeutics.

Received: January 7, 2014
Revised: March 4, 2014
Accepted: March 19, 2014
Published: May 1, 2014

REFERENCES

Ala, U., Karreth, F.A., Bosia, C., Pagnani, A., Taulli, R., Léopold, V., Tay, Y., Provero, P., Zecchina, R., and Pandolfi, P.P. (2013). Integrated transcriptional and competitive endogenous RNA networks are cross-regulated in permissive molecular environments. Proc. Natl. Acad. Sci. USA *110*, 7154–7159.

Ameres, S.L., Horwich, M.D., Hung, J.H., Xu, J., Ghildiyal, M., Weng, Z., and Zamore, P.D. (2010). Target RNA-directed trimming and tailing of small silencing RNAs. Science *328*, 1534–1539.

Arvey, A., Larsson, E., Sander, C., Leslie, C.S., and Marks, D.S. (2010). Target mRNA abundance dilutes microRNA and siRNA activity. Mol. Syst. Biol. *6*, 363.

Baek, D., Villén, J., Shin, C., Camargo, F.D., Gygi, S.P., and Bartel, D.P. (2008). The impact of microRNAs on protein output. Nature *455*, 64–71.

Bissels, U., Wild, S., Tomiuk, S., Holste, A., Hafner, M., Tuschl, T., and Bosio, A. (2009). Absolute quantification of microRNAs by using a universal reference. RNA *15*, 2375–2384.

Brenner, J.L., Jasiewicz, K.L., Fahley, A.F., Kemp, B.J., and Abbott, A.L. (2010). Loss of individual microRNAs causes mutant phenotypes in sensitized genetic backgrounds in *C. elegans*. Curr. Biol. *20*, 1321–1325.

Cesana, M., Cacchiarelli, D., Legnini, I., Santini, T., Sthandier, O., Chinappi, M., Tramontano, A., and Bozzoni, I. (2011). A long noncoding RNA controls muscle differentiation by functioning as a competing endogenous RNA. Cell *147*, 358–369.

Channon, H.J., and Wilkinson, H. (1936). The effect of various fats in the production of dietary fatty livers. Biochem. J. *30*, 1033–1039.

Coelho, T., Adams, D., Silva, A., Lozeron, P., Hawkins, P.N., Mant, T., Perez, J., Chiesa, J., Warrington, S., Tranter, E., et al. (2013). Safety and efficacy of RNAi therapy for transthyretin amyloidosis. N. Engl. J. Med. *369*, 819–829.

Ebert, M.S., Neilson, J.R., and Sharp, P.A. (2007). MicroRNA sponges: competitive inhibitors of small RNAs in mammalian cells. Nat. Methods *4*, 721–726.

Esau, C., Davis, S., Murray, S.F., Yu, X.X., Pandey, S.K., Pear, M., Watts, L., Booten, S.L., Graham, M., McKay, R., et al. (2006). miR-122 regulation of lipid metabolism revealed by in vivo antisense targeting. Cell Metab. *3*, 87–98.

Eulalio, A., Huntzinger, E., and Izaurralde, E. (2008). Getting to the root of miRNA-mediated gene silencing. Cell *132*, 9–14.

Fang, L., Du, W.W., Yang, X., Chen, K., Ghanekar, A., Levy, G., Yang, W., Yee, A.J., Lu, W.Y., Xuan, J.W., et al. (2013). Versican 3′-untranslated region (3′-UTR) functions as a ceRNA in inducing the development of hepatocellular carcinoma by regulating miRNA activity. FASEB J. *27*, 907–919.

Farh, K.K., Grimson, A., Jan, C., Lewis, B.P., Johnston, W.K., Lim, L.P., Burge, C.B., and Bartel, D.P. (2005). The widespread impact of mammalian MicroRNAs on mRNA repression and evolution. Science *310*, 1817–1821.

Figliuzzi, M., Marinari, E., and De Martino, A. (2013). MicroRNAs as a selective channel of communication between competing RNAs: a steady-state theory. Biophys. J. *104*, 1203–1213.

Franco-Zorrilla, J.M., Valli, A., Todesco, M., Mateos, I., Puga, M.I., Rubio-Somoza, I., Leyva, A., Weigel, D., García, J.A., and Paz-Ares, J. (2007). Target mimicry provides a new mechanism for regulation of microRNA activity. Nat. Genet. *39*, 1033–1037.

Friedman, R.C., Farh, K.K.H., Burge, C.B., and Bartel, D.P. (2009). Most mammalian mRNAs are conserved targets of microRNAs. Genome Res. *19*, 92–105.

Garcia, D.M., Baek, D., Shin, C., Bell, G.W., Grimson, A., and Bartel, D.P. (2011). Weak seed-pairing stability and high target-site abundance decrease the proficiency of lsy-6 and other microRNAs. Nat. Struct. Mol. Biol. *18*, 1139–1146.

Giraldez, A.J., Mishima, Y., Rihel, J., Grocock, R.J., Van Dongen, S., Inoue, K., Enright, A.J., and Schier, A.F. (2006). Zebrafish MiR-430 promotes deadenylation and clearance of maternal mRNAs. Science *312*, 75–79.

Grimson, A., Farh, K.K., Johnston, W.K., Garrett-Engele, P., Lim, L.P., and Bartel, D.P. (2007). MicroRNA targeting specificity in mammals: determinants beyond seed pairing. Mol. Cell *27*, 91–105.

Guo, H., Ingolia, N.T., Weissman, J.S., and Bartel, D.P. (2010). Mammalian microRNAs predominantly act to decrease target mRNA levels. Nature *466*, 835–840.

Hafner, M., Landthaler, M., Burger, L., Khorshid, M., Hausser, J., Berninger, P., Rothballer, A., Ascano, M., Jr., Jungkamp, A.C., Munschauer, M., et al. (2010). Transcriptome-wide identification of RNA-binding protein and microRNA target sites by PAR-CLIP. Cell *141*, 129–141.

Hansen, T.B., Jensen, T.I., Clausen, B.H., Bramsen, J.B., Finsen, B., Damgaard, C.K., and Kjems, J. (2013). Natural RNA circles function as efficient microRNA sponges. Nature *495*, 384–388.

Ishibashi, S., Brown, M.S., Goldstein, J.L., Gerard, R.D., Hammer, R.E., and Herz, J. (1993). Hypercholesterolemia in low density lipoprotein receptor knockout mice and its reversal by adenovirus-mediated gene delivery. J. Clin. Invest. *92*, 883–893.

Jeyapalan, Z., Deng, Z., Shatseva, T., Fang, L., He, C., and Yang, B.B. (2011). Expression of CD44 3′-untranslated region regulates endogenous microRNA functions in tumorigenesis and angiogenesis. Nucleic Acids Res. *39*, 3026–3041.

Jopling, C.L., Yi, M., Lancaster, A.M., Lemon, S.M., and Sarnow, P. (2005). Modulation of hepatitis C virus RNA abundance by a liver-specific MicroRNA. Science *309*, 1577–1581.

Karreth, F.A., Tay, Y., Perna, D., Ala, U., Tan, S.M., Rust, A.G., DeNicola, G., Webster, K.A., Weiss, D., Perez-Mancera, P.A., et al. (2011). In vivo identification of tumor- suppressive PTEN ceRNAs in an oncogenic BRAF-induced mouse model of melanoma. Cell *147*, 382–395.

Krützfeldt, J., Rajewsky, N., Braich, R., Rajeev, K.G., Tuschl, T., Manoharan, M., and Stoffel, M. (2005). Silencing of microRNAs in vivo with 'antagomirs'. Nature *438*, 685–689.

Landgraf, P., Rusu, M., Sheridan, R., Sewer, A., Iovino, N., Aravin, A., Pfeffer, S., Rice, A., Kamphorst, A.O., Landthaler, M., et al. (2007). A mammalian microRNA expression atlas based on small RNA library sequencing. Cell *129*, 1401–1414.

Lewis, B.P., Burge, C.B., and Bartel, D.P. (2005). Conserved seed pairing, often flanked by adenosines, indicates that thousands of human genes are microRNA targets. Cell *120*, 15–20.

Li, X., Cassidy, J.J., Reinke, C.A., Fischboeck, S., and Carthew, R.W. (2009). A microRNA imparts robustness against environmental fluctuation during development. Cell *137*, 273–282.

Lujambio, A., and Lowe, S.W. (2012). The microcosmos of cancer. Nature *482*, 347–355.

Memczak, S., Jens, M., Elefsinioti, A., Torti, F., Krueger, J., Rybak, A., Maier, L., Mackowiak, S.D., Gregersen, L.H., Munschauer, M., et al. (2013). Circular RNAs are a large class of animal RNAs with regulatory potency. Nature *495*, 333–338.

Mendell, J.T., and Olson, E.N. (2012). MicroRNAs in stress signaling and human disease. Cell *148*, 1172–1187.

Mukherji, S., Ebert, M.S., Zheng, G.X., Tsang, J.S., Sharp, P.A., and van Oudenaarden, A. (2011). MicroRNAs can generate thresholds in target gene expression. Nat. Genet. *43*, 854–859.

Mullokandov, G., Baccarini, A., Ruzo, A., Jayaprakash, A.D., Tung, N., Israelow, B., Evans, M.J., Sachidanandam, R., and Brown, B.D. (2012). High-throughput assessment of microRNA activity and function using microRNA sensor and decoy libraries. Nat. Methods *9*, 840–846.

Pillai, R.S., Bhattacharyya, S.N., Artus, C.G., Zoller, T., Cougot, N., Basyuk, E., Bertrand, E., and Filipowicz, W. (2005). Inhibition of translational initiation by Let-7 MicroRNA in human cells. Science *309*, 1573–1576.

Poliseno, L., Salmena, L., Zhang, J., Carver, B., Haveman, W.J., and Pandolfi, P.P. (2010). A coding-independent function of gene and pseudogene mRNAs regulates tumour biology. Nature *465*, 1033–1038.

Rhodes, D.R., and Chinnaiyan, A.M. (2005). Integrative analysis of the cancer transcriptome. Nat. Genet. Suppl. *37*, S31–S37.

Salmena, L., Poliseno, L., Tay, Y., Kats, L., and Pandolfi, P.P. (2011). A ceRNA hypothesis: the Rosetta Stone of a hidden RNA language? Cell *146*, 353–358.

Seitz, H. (2009). Redefining microRNA targets. Curr. Biol. *19*, 870–873.

Tay, Y., Kats, L., Salmena, L., Weiss, D., Tan, S.M., Ala, U., Karreth, F., Poliseno, L., Provero, P., Di Cunto, F., et al. (2011). Coding-independent regulation of the tumor suppressor PTEN by competing endogenous mRNAs. Cell *147*, 344–357.

Tsai, W.C., Hsu, P.W., Lai, T.C., Chau, G.Y., Lin, C.W., Chen, C.M., Lin, C.D., Liao, Y.L., Wang, J.L., Chau, Y.P., et al. (2009). MicroRNA-122, a tumor suppressor microRNA that regulates intrahepatic metastasis of hepatocellular carcinoma. Hepatology *49*, 1571–1582.

Wee, L.M., Flores-Jasso, C.F., Salomon, W.E., and Zamore, P.D. (2012). Argonaute divides its RNA guide into domains with distinct functions and RNA-binding properties. Cell *151*, 1055–1067.

Zhang, W., Sargis, R.M., Volden, P.A., Carmean, C.M., Sun, X.J., and Brady, M.J. (2012). PCB 126 and other dioxin-like PCBs specifically suppress hepatic PEPCK expression via the aryl hydrocarbon receptor. PLoS ONE *7*, e37103.

Molecular Cell, Volume *54*

Supplemental Information

Assessing the ceRNA Hypothesis with Quantitative Measurements of miRNA and Target Abundance

Rémy Denzler, Vikram Agarwal, Joanna Stefano, David P. Bartel, and Markus Stoffel

Figure S1
Denzler et al.

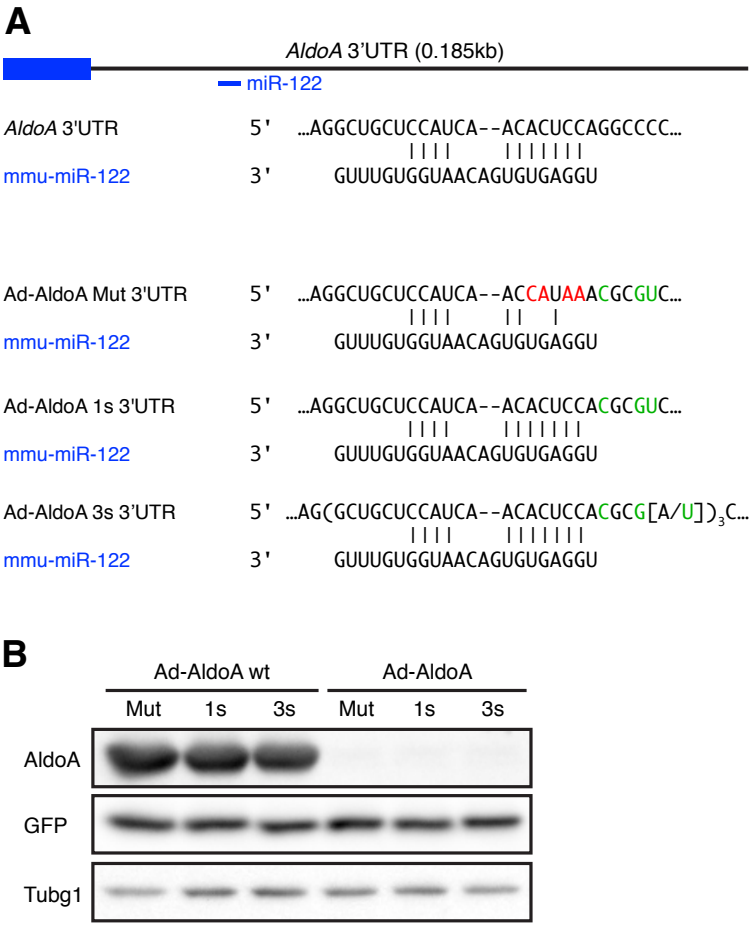

Figure S1: *AldoA* miR-122 sites and adenovirus characterization. Related to Figure 1.

(A) Position and complementarity of the miR-122 binding site within the mouse *AldoA* 3′UTR (top) and the respective site(s) within the Ad-AldoA adenoviruses (bottom). Mutations in the seed match are shown in red, and additional differences compared to the endogenous *AldoA* 3′UTR are in green. **(B)** Western blot of primary hepatocytes infected with Ad-AldoA and Ad-AldoA expressing the full-length protein (Ad-AldoA-wt) with a mutated (Mut), one (1s) or three (3s) miR-122 binding site(s) at MOI 200.

Figure S2
Denzler et al.

A

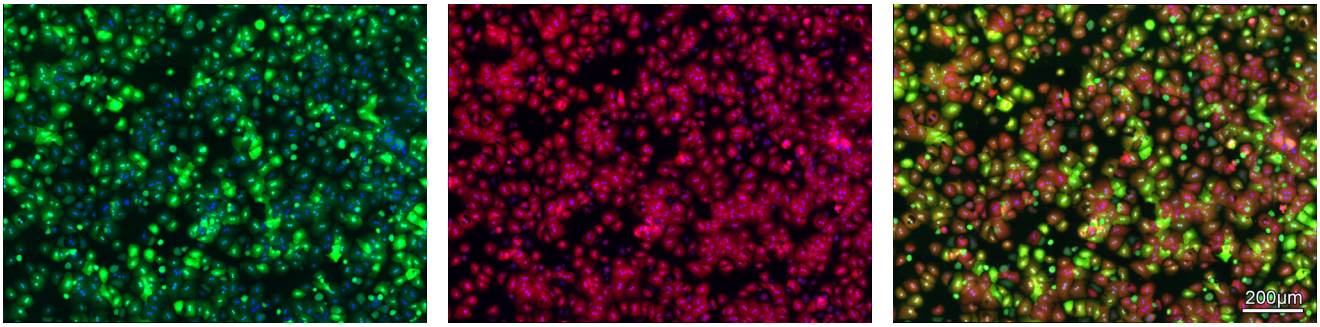

B

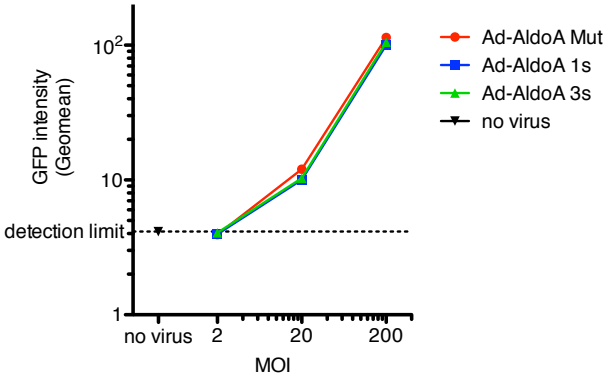

C

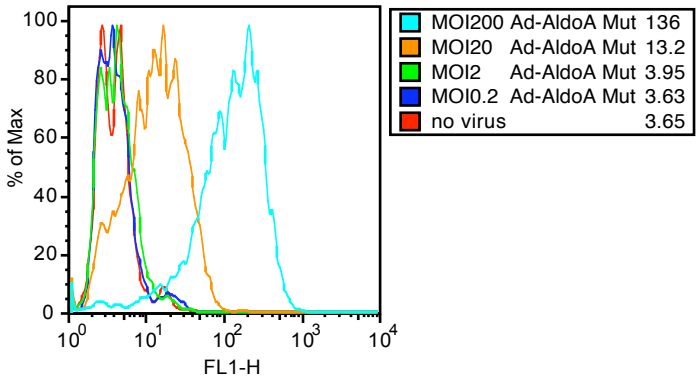

D

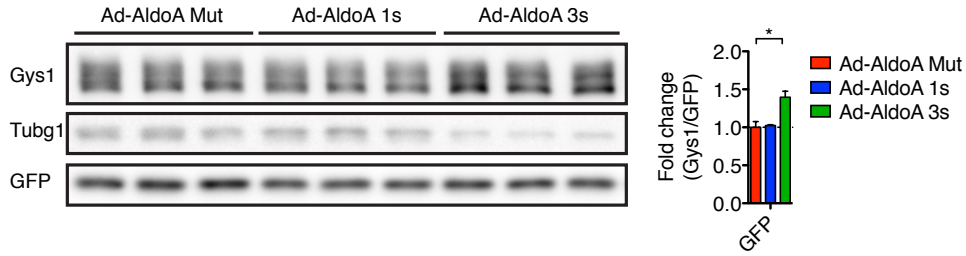

Figure S2: Analysis of adenovirus infection of primary hepatocytes. Related to Figure 1.

(A) Representative light microscopy image of primary hepatocytes infected with Ad-Ctrl at MOI 200 showing nuclear Hoechst 33342 staining (all pictures), viral GFP expression (green, left picture), cytoplasm staining (red, middle picture) and merge (right picture).

(B) Absolute quantification of GFP intensity of primary hepatocytes infected with Ad-AldoA with one (1s), three (3s) or a mutated (Mut) miR-122 binding site at MOI 0.2, 2, 20 or 200 and no virus. Data represent mean ± SEM (n = 3).

(C) Representative histogram showing flow cytometry data for the Ad-AldoA Mut at the indicated MOIs. Numbers at the right of the key indicate geomean intensity values.

(D) Western blot and respective quantification showing levels of proteins detected in primary hepatocytes infected with Ad-AldoA constructs at MOI 200. Data represent mean ± SEM (n = 3). *P < 0.05, unpaired t test.

Figure S3
Denzler et al.

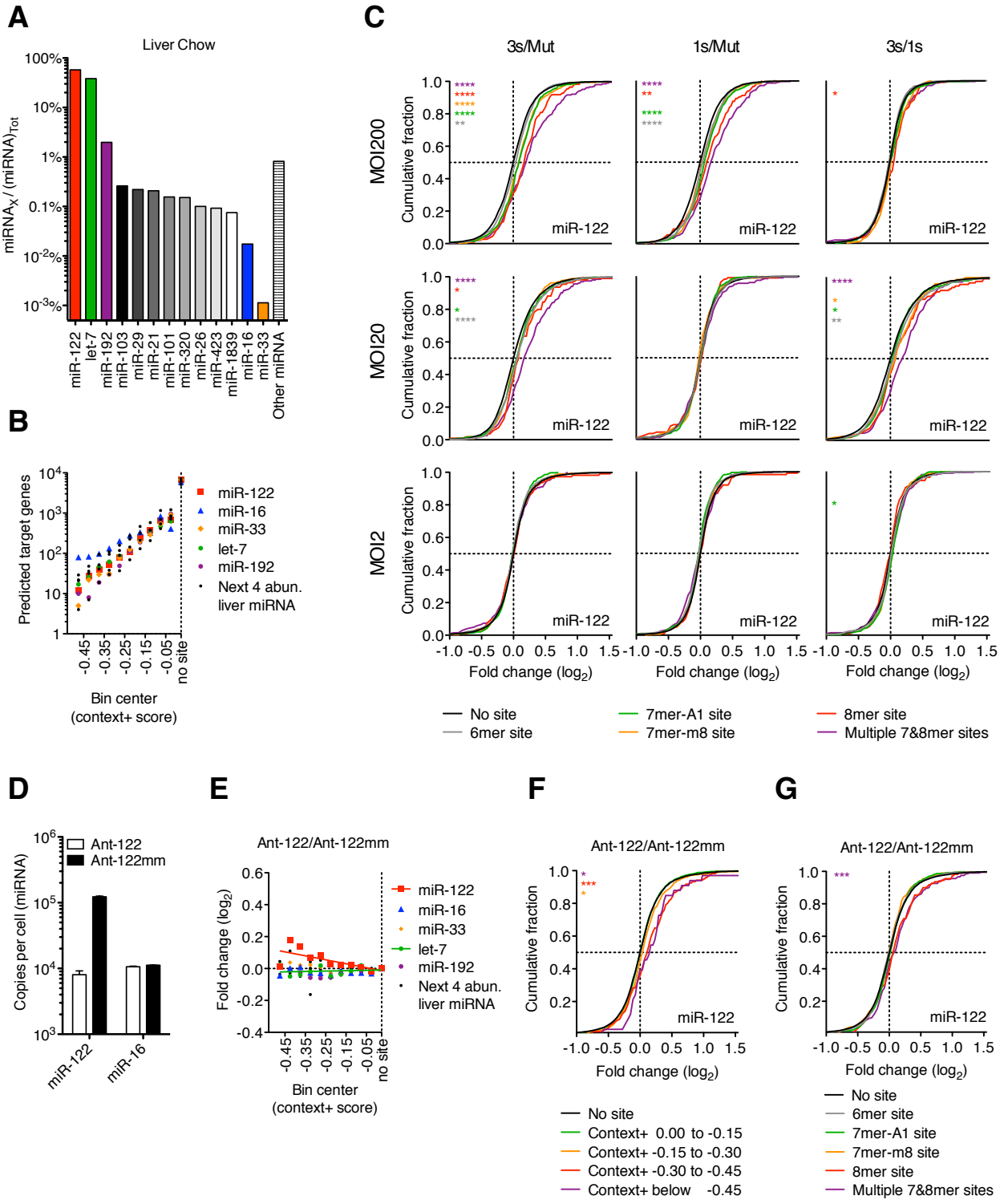

Figure S3: Amount of derepression correlates with predicted site efficacy and number of added *AldoA* MREs. Related to Figure 3.

(A) Relative expression miRNA families in wildtype livers as indicated by small-RNA sequencing. Represented are the 11 miRNA families most abundant in liver, plus miR-16 and miR-33.

(B) Number of predicted targets for the indicated miRNAs in each bin of Figure 4A.

(C) RNA-seq data from primary hepatocytes infected with MOI 2, 20 and 200 of Ad-AldoA Mut, 1s or 3s shown in Figure 1C-H and Figure 4B. Cumulative distributions of mRNA changes for genes with no miR-122 site (black) or predicted target genes with the indicated site type (color). Number of genes per bin: no site, 6444; 6mer, 1001; 7mer-A1, 398; 7mer-m8, 269; 8mer, 110; multiple, 203. *P < 0.05, **P < 0.01, ***P < 0.001, ****, P < 0.0001, one-sided Kolmogorov–Smirnov (K–S) test.

(D) miRNA molecules in primary hepatocytes treated with Ant-122 or Ant-122mm. Mean ± SEM (n = 3).

(E) RNA-seq results from primary hepatocytes of (D) showing mRNA changes of predicted targets after inhibiting miR-122. Predicted targets of miR-122 (red), miR-16 (blue), miR-33 (orange), let-7 (green), miR-192 (purple), or a combination of the next four most abundant liver miRNA families (black) were grouped into ten bins based on their context+ scores. For each miRNA family, the median $\log_2$-fold change is plotted for the predicted targets in each bin. Medians were normalized to that of the bin with genes without sites. Each bin had at least 10 genes; see (B) for group sizes.

(F) Cumulative distributions of mRNA changes in the hepatocytes of (D) for genes with no miR-122 site (black) or predicted target genes with the indicated context+ score bins (color). Number of genes per bin: black, 6629; green, 1693; orange, 434; red, 120; purple, 33. *P < 0.05, **P < 0.01, ***P < 0.001, ****, P <0.0001, one-sided K–S test.

(G) Cumulative distributions of mRNA changes in the hepatocytes of (D) for genes with no miR-122 site (black) or predicted target genes with the indicated sites (color). Otherwise, as in (C).

Figure S4
Denzler et al.

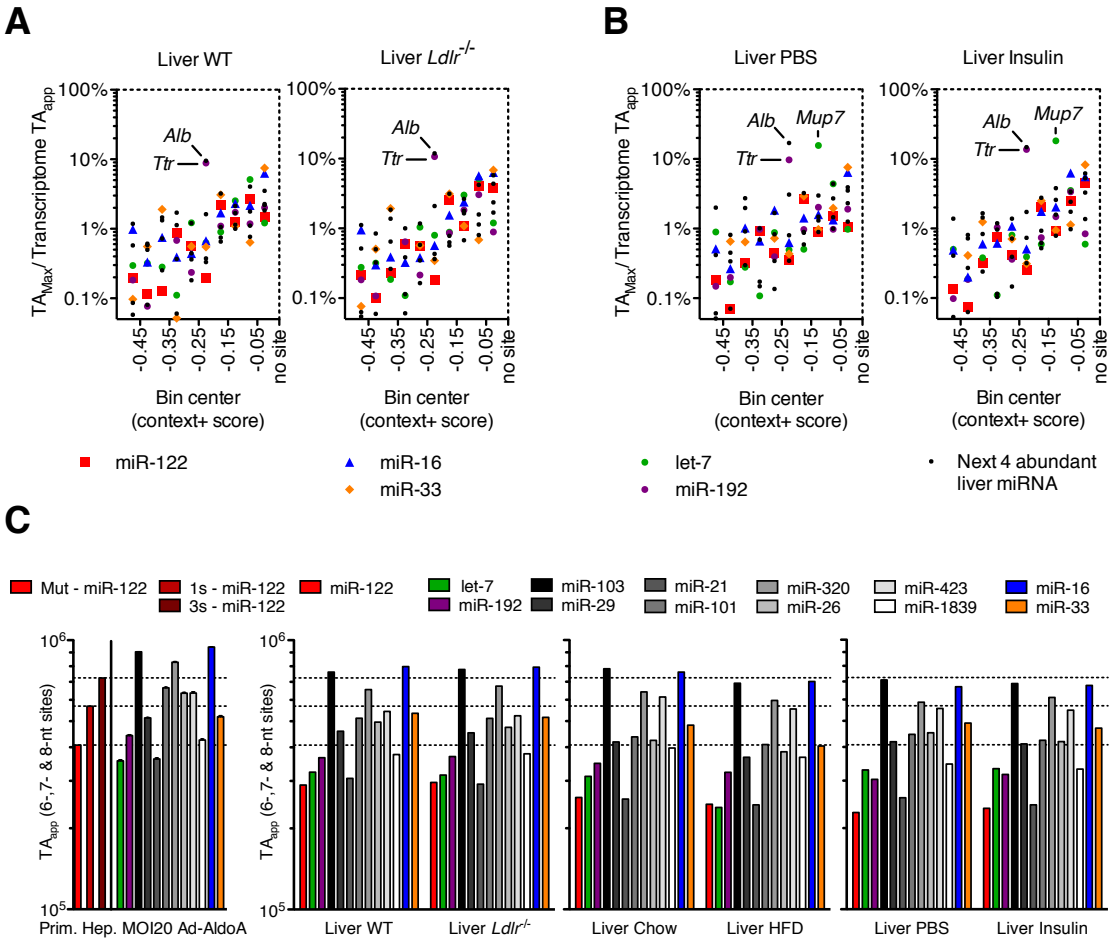

Figure S4: Modest changes in target abundance induced by metabolic stress and disease. Related to Figure 4.

(A–B) Fractional contribution of the largest potential contributors to transcriptome TA_{app} in livers originated from *Ldlr*$^{-/-}$ or wildtype (WT) mice **(A)** or in livers that originated from wildtype mice perfused either with Insulin or PBS **(B)**. Potential contributors were binned by their context+ score, and the top potential contributors are plotted within each bin.

(C) Transcriptome TA_{app} in primary hepatocytes (n = 3) infected with MOI 20 Ad-AldoA or in livers (n = 1) from models of physiological (Insulin) or disease/stress states (*Ldlr*$^{-/-}$ and HFD). Dashed lines indicate miR-122 TA_{app} at MOI 20 of Ad-AldoA Mut, 1s, and 3s.

Table S1: Gene expression levels, fold-changes, and predicted target site efficacy scores (context+ scores) across all hepatocyte RNA-seq samples. Related to Figure 3 and S3).

Table S2: Gene expression levels, fold-changes, and predicted target site efficacy scores (context+ scores) across all liver RNA-seq samples. Related to Figure 4 and S4).

Table S3: Primer sets used in this study

Name	Sequence (5' to 3')
P1 (AldoA 5'UTR)	CAGCTGAATAGGCTGCGTTC
P2 (AldoA 3'UTR)	TTTTTCCCCCTTAAATAGTTGTT
P3 (AldoA MluI site f)	CTCCATCAACACTCCACGCGTCTGCCTACCCACTTGC
P4 (AldoA MluI site r)	GCAAGTGGGTAGGCAGACGCGTGGAGTGTTGATGGAG
P5 (AldoA Mut MluI site f)	AGCTGAACTAAGGCTGCTCCATCAACCATAAACGCGTCTGCCTACCCACT TGCTATTGAAGA
P6 (AldoA Mut MluI site r)	CTCTTCAATAGCAAGTGGGTAGGCAGACGCGTTTATGGTTGATGGAGCAG CCTTAGTTCAGCT
P7 (AldoA miR-122 sites f)	CGCGAGCTGCTCCATCAACACTCCACGCGAGCTGCTCCATCAACACTCCA
P8 (AldoA miR-122 sites r)	CGCGTGGAGTGTTGATGGAGCAGCTCGCGTGGAGTGTTGATGGAGCAGCT
P9 (AldoA Stop f)	CAGCTCCTTCTTCTGCTCTCAGGTCAGTGCTGGGTATGG
P10 (AldoA Stop r)	CCATACCCAGCACTGACCTGAGAGCAGAAGAAGGAGCTG
36B4 f	GCCGTGATGCCCAGGGAAGACA
36B4 r	CATCTGCTTGGAGCCCACGTTG
AldoA f	GCGCTGTGTGCTAAAGATTG
AldoA r	AGGCTCCACAATGGGTACAA
GFP f	GAAGCGCGATCACATGGT
GFP r	CCATGCCGAGAGTGATCC
Gys1 f	GGTGTGAGGACGCAGGTAG
Gys1 r	GCCAACGCCCAAAATACA
Slc7a1 f	ATTTCAGCCGGCCTCCTA
Slc7a1 r	TGCCCACAGTGTCCCTTC
P4ha1 f	CGTGGGGAGGGTATCAAAAT
P4ha1 r	ATGGTAGCGGCAGAACAGTC
Ndrg3 f	TCCTGGCCAACAAGAAGC
Ndrg3 r	CTCATCCATGGTGGGGTACT
Tmed3 f	GGTCACGGCTCTCACTCAG
Tmed3 r	TCACAGTCTTCAGAGCCTCGT
Snrk f	TGCGGGTCTCTTGCATACT
Snrk r	GCCCAGGCTCCATATGTCTA
Dyrk2 f	CTACCACTACAGCCCACACG
Dyrk2 r	TCTGTCCGTGGCTGTTGA
ApoM f	CCCAGACATGAAAACAGACCT
ApoM r	GGGTGTGGTGACCGATTG
Crot f	AGTGAAGGGCATTGTCCAAC
Crot r	TCTTGTGGATATATGTCAATTGTCTG
Chka f	AACAGATTTGCTCTTGCCTCTC
Chka r	TCAAAGTAGGCCTCGAATCTG

EXTENDED EXPERIMENTAL PROCEDURES

Animal Experiments

Animals were maintained on a 12-hour light/dark cycle under a controlled environment in a pathogen-free facility at the Institute for Molecular Systems Biology, ETH Zürich (Switzerland). The *Ldlr* KO mice were originally obtained from the Jackson Laboratory (B6.129S7-*Ldlrtm1Her*/J) and backcrossed for >10 generations into a *C57Bl/6J* background. For the liver insulin perfusion experiments, starved *C57Bl/6J* mice were euthanized and the portal vein was canulated. The liver was perfused with oxygenated Krebs–Henseleit buffer with 0 or 20 ng/ml insulin at 37 °C in a single-pass mode with a total flow rate of 1.5 to 2 ml min^{-1} for 4 hours (Wolfrum et al., 2004). All animal experiments were approved by the ethics committee of the Kantonale Veterinäramt Zürich.

Primary Hepatocytes Isolation and Viral Infections

Primary hepatocytes were isolated based on the method described by Zhang et al. (Zhang et al., 2012) with the following modifications and conditions (additional explanations, images, and videos to primary hepatocyte isolation can be found on http://www.mouselivercells.com). Male 8- to 12-week-old C57BL/6N mice (Charles River) were anesthetized by intraperitoneal injection of 150 ul pentobarbital (Esconarkon US vet) pre-diluted 1:5 in PBS. The liver was perfused by cannulation of the caudal vena cava with the portal vein as a drain. The liver was perfused with pre-warmed Hank's Balanced Salt Solution (Life Technologies) containing 0.5 mM EGTA followed by pre-warmed digestion medium [DMEM 1 g/l glucose (Life Technologies) supplemented with 1% Penicillin-Streptomycin (Life Technologies), 15mM HEPES (Life Technologies) and 30 ug/ml Liberase TM Research Grade medium Thermolysin concentration (Roche)] each for four minutes with a flow rate of 3 ml min^{-1}. The liver was surgically removed, hepatocytes released into 10 ml digestion media by shaking and supplemented with 15 ml ice cold low glucose media [DMEM 1 g/l glucose (Life Technologies) supplemented with 1% Penicillin-Streptomycin (Life Technologies), 10% heat-inactivated fetal bovine serum (Sigma) and 1% Glutamax (Life Technologies)] and filtered through a 100 um Cell Strainer (BD). The suspension was then washed three times with 25 ml of ice-cold low glucose media (50g at 4°C for 2 min). Hepatocytes were counted and plated at 300,000 cells/well in surface-treated 6-well plates (BD Primaria) in low glucose media. 4–6 hours after plating, cells were infected with adenovirus constructs in Hepatozyme media [HepatoZYME-SFM (Life Technologies) supplemented with 1% Penicillin-Streptomycin (Life Technologies),

1% Glutamax (Life Technologies)] and harvested 24 hours post infection. All cells were incubated at 37°C in a humidified atmosphere containing 5% CO_2.

RNA Isolation

RNA was extracted using Trizol (Life Technologies) according to the manufacturer's instructions, except for a 30 min isopropanol precipitation at –20°C. RNA integrity was analyzed on an Agilent 2100 Bioanalyzer for all samples that were sequenced.

Cell Number Calculation

By dividing total RNA yield from one 6-well plate well (22 ug RNA) by the cell number obtained from microscopy (300,000 cells per 6-well plate well), one hepatocyte was calculated to yield 73.5 pg RNA.

Gene Expression Analysis

2 ug of total RNA was treated with the DNA-free Kit (Life Technologies) and reverse-transcribed using the High Capacity cDNA Reverse Transcription Kit (Life Technologies). Quantitative PCR reactions were performed with the Light Cycler 480 (Roche) employing a 384-well format, gene-specific primer pairs (see Table S3, designed by http://qpcr.probefinder.com/organism.jsp) and KAPA SYBR Fast qPCR Master Mix (2x) for LightCycler 480 (Kapa Biosystems). Cycles were quantified employing Light Cycler 480 Analysis Software (Abs quantification/ 2^{nd} derivate max). Relative gene expression was calculated using the ddCT method and mouse *36b4* (*Rplp0*) for normalization. For absolute mRNA quantification the pCR2.1 plasmids of AldoA and the coding regions of Carnitine O-octanoyltransferase (*Crot*, NM_023733.3), Choline Kinase alpha (*Chka*, NM_013490) and Apolipoprotein M (*ApoM*, NM_018816) were cloned into plasmids with a T7 promoter. All plasmids were linearized after the poly-A region, transcribed using the T7 Quick High Yield RNA Synthesis Kit (NEB), cleaned up using the RNAeasy MinElute Cleanup Kit (Qiagen), and visualized on a gel to confirm the presence and correct size of the RNA. Molar concentrations of mRNA transcripts were quantified using a NanoDrop ND-1000 spectrophotometer (Thermo Scientific) and the respective molecular weight. To create a standard curve, the mRNA transcripts were serial diluted, spiked into 2 ug of yeast RNA, reverse transcribed and quantified by PCR performed as described above.

miRNA Expression Analysis

150 ng of total RNA was reverse-transcribed using TaqMan MicroRNA Assays (Life Technologies) and TaqMan MicroRNA Reverse Transcription Kit (Life Technologies). The RT primers were multiplexed in a dilution of 1:20 as described by the manufacturer. Quantitative PCR reactions were performed with the Light Cycler 480 (Roche) employing a 384-well format, TaqMan Universal PCR Master Mix, No AmpErase UNG (Life Technologies) and TaqMan MicroRNA Assays (Life Technologies). Cycles were quantified employing Light Cycler 480 analysis software (Abs quantification/ 2^{nd} derivate max). Relative miRNA expression was calculated using the ddCT method and mouse snoRNA202 for normalization. For absolute quantification synthetic miRNAs (Sigma-Aldrich) were quantified using a NanoDrop ND-1000 spectrophotometer (Thermo Scientific) and the respective molecular weight. miRNAs were spiked into primary hepatocyte cell lysates and absolutely quantified employing a synthetic miRNA standard curve.

Small RNA sequencing and data analysis

For small-RNA libraries (performed by BGI): Total RNA was size fractionated (18–30 nt), followed by 5′ and 3′ adaptor ligations, RT-PCR, and Solexa sequencing. To quantify miRNA levels, we counted the number of occurrences in which the first 20 nt of the raw sequence matched a known mature *Mus musculus* miRNA sequence deposited in miRBase version 20.

RNA-seq data analysis

To process RNA-seq data, raw reads were aligned to the latest build of the mouse genome (mm10) using STAR v. 2.3.1n (options --outFilterType BySJout --outFilterMultimapScoreRange 0 --readMatesLengthsIn Equal --outFilterIntronMotifs RemoveNoncanonicalUnannotated --clip3pAdapterSeq TCGTATGCCGTCTTCTGCTTG --outStd SAM) (Dobin et al., 2013). The option "--clip3pNbases 2" was additionally used for the libraries with the following codes: ACAGTG-s_6, CAGATC-s_6, CGATGT-s_6, CTTGTA-s_6, GCCAAT-s_6, TGACCA-s_6 due to sequencing errors in the last 2 nucleotides. Pooling all biological replicates of a particular sample, differential expression analysis was performed between two samples of interest using cuffdiff v. 2.1.1 (options --library-type fr-firststrand -b mm10.fa -u --max-bundle-frags 100000000) (Trapnell et al., 2013), using mouse transcript models of protein-coding and long noncoding RNA genes annotated in Ensembl release 72. For data analysis, only genes with FPKM

above 1.0 were considered. Raw files as well as processed files for gene expression measurements and differential expression analysis are deposited in the GEO (accession ID GSE52801).

Target Abundance Calculation

We fit a linear regression function to transform gene expression measurements (measured in FPKM) from RNA-seq data into absolute copy numbers (as determined by quantitative PCR) (Figure 4A). To account for experimental noise in qPCR and RNA-seq measurements, we used the constraints that there be no x or y weighting and that the y intercept equal 0. Copy numbers per cell were determined by multiplying the FPKM with the resulting slope of 3.83. For each miRNA, the copy number of each predicted target gene was weighted by the number of 6-, 7-, and 8-nt 3′UTR binding sites, and these values were summed to yield TA_{app}.

Generation of adenovirus construct

AldolaseA variant 2 (*AldoA*, NM_007438) was amplified from cDNA with primers P1 and P2 (Table S3) using platinum PCR SuperMix High Fidelity (Life Technologies) and brought into the plasmid PCR 2.1-TOPO (pCR2.1) vector using TOPO TA Cloning Kit (Life Technologies). An MluI restriction site was introduced after the miR-122 binding site (Aldo 1s wt) using QuickChange II Site-Directed Mutagenesis Kit (Agilent) and primers P3 and P4. Analogously an MluI restriction site along with mutations in the seed target region of miR-122 at positions 2, 3, 5 and 6 (Aldo Mut wt) using the primers P5 and P6 were inserted. Two additional miR-122 binding sites were introduced into Aldo 1s wt by inserting a synthetic linker resulting in Aldo 3s wt. The plasmid pCR2.1 Aldo 1s wt was digested with MluI (NEB), dephosphorylated using Antarctic Phosphatase (NEB) and cleaned up with QIAaquick Gel Extraction Kit (Qiagen). For the synthetic linkers an unimolar mixture of linker oligonucleotite P7 and P8 with two miR-122 binding sites were first denatured at 95°C for 5 minutes, annealed by lowering the temperature from 70°C for 10 minutes followed by 60°C, 50°C, 40°C, and 20°C for 3 minutes each (using a ramping temperature of 0.07°C/s) and phosphorylated using T4 Polynucleotide Kinase (NEB). The linker and pCR2.1 Aldo 1s wt backbone were then ligated at room temperature for 1 hour using T4 DNA Ligase (NEB), transformed in Mach1 cells (Life Technologies), screened for insertion length and then sequenced. The three plasmids (pCR2.1 Aldo Mut wt, 1s wt, and 3s wt) were then re-cloned into pVQAd CMV K-NpA (pVQAd, Viraquest) using the restriction sites BamHI and XhoI (NEB). Finally, a stop codon was introduced at amino acid position ten using QuickChange II Site-Directed Mutagenesis Kit

(Agilent), primers P9 and P10 and plasmids pVQAd Aldo Mut wt, 1s wt, and 3s wt resulting in plasmids pVQAd Aldo Mut, 1s, and 3s. All pVQAd plasmids constructs were sent for adenovirus production to Viraquest Inc., USA.

Antibodies

Antibodies used for Immunoblotting: AldoA (rabbit, 1:1000, Cell Signaling, #3188), GFP (rabbit, 1:1000; Life Technologies, A11122), Tubg1 (mouse, 1:5000, Sigma-Aldrich, T6557), Gys1 (rabbit, 1:300, Cell Signaling, #3893).

Immunoblotting

Cells were lysed with 250 ul RIPA lysis buffer (50 mmol/l Tris-HCl pH 7.5, 150 mmol/l NaCl, 2 mmol/l EDTA, 1% NP-40, 1% sodium deoxycholate, 1% triton-X 100 and protease inhibitor cocktail) for 5 min on ice. Protein concentration was determined using the Bicinchoninic Acid Kit (Sigma-Aldrich). Equal protein amounts were boiled in Laemmli buffer (1.7% SDS, 5% glycerol, 0.002% bromophenol blue, 60 mM Tris-HCl pH 6.8, 100 mM DTT) for 5 min at 98°C, separated by 12% SDS-PAGE and transferred onto nitrocellulose membranes by electroblotting in a wet chamber (Bio-Rad). The membranes were blocked for one hour with 5% non-fat dry milk TBS-0.1% Tween (Sigma-Aldrich), incubated with the primary antibodies overnight at 4°C, followed by a one hour incubation with a horseradish peroxidase-conjugated secondary antibody (Calbiochem). Blots were then developed by chemiluminescent detection with a Fujifilm analyzer (LAS-4000) and quantified using ImageJ (Schneider et al., 2012).

Immunohistochemistry

Cells were fixed on ice for 45 min with 4% paraformaldehyde, permeabilized for 15 min at room temperature with PBS containing 0.1% Triton-X and stained with PBS containing 1:10’000 HCS CellMask Red stain (Life Technologies) and 1:2000 Hoechst 33342 (Life Technologies) for 30 min at room temperature. Plates were imaged with Zeiss Axio Observer Z1 at 20x magnification and cell numbers assessed using cell profiler software (Kamentsky et al., 2011).

Flow cytometry

Primary hepatocytes were trypsinized, fixed at room temperature for 15 min with 4% paraformaldehyde and resuspended in FACS buffer (2% FBS, 5 mM EDTA, and 0.02% NaN3 in PBS). Samples were analyzed counting 10,000 events per sample using a BD FACSCalibur flow cytometer and the FlowJo software package.

Plasma cholesterol levels

Cholesterol was measured from mouse serum using a commercial kit (Roche Diagnostics).

SUPPLEMENTAL REFERENCES

Dobin, A., Davis, C.A., Schlesinger, F., Drenkow, J., Zaleski, C., Jha, S., Batut, P., Chaisson, M., and Gingeras, T.R. (2013). STAR: ultrafast universal RNA-seq aligner. Bioinformatics *29*, 15-21.

Kamentsky, L., Jones, T.R., Fraser, A., Bray, M.A., Logan, D.J., Madden, K.L., Ljosa, V., Rueden, C., Eliceiri, K.W., and Carpenter, A.E. (2011). Improved structure, function and compatibility for CellProfiler: modular high-throughput image analysis software. Bioinformatics *27*, 1179-1180.

Schneider, C.A., Rasband, W.S., and Eliceiri, K.W. (2012). NIH Image to ImageJ: 25 years of image analysis. Nat Methods *9*, 671-675.

Trapnell, C., Hendrickson, D.G., Sauvageau, M., Goff, L., Rinn, J.L., and Pachter, L. (2013). Differential analysis of gene regulation at transcript resolution with RNA-seq. Nature Biotechnology *31*, 46-+.

Wolfrum, C., Asilmaz, E., Luca, E., Friedman, J.M., and Stoffel, M. (2004). Foxa2 regulates lipid metabolism and ketogenesis in the liver during fasting and in diabetes. Nature *432*, 1027-1032.

Zhang, W., Sargis, R.M., Volden, P.A., Carmean, C.M., Sun, X.J., and Brady, M.J. (2012). PCB 126 and other dioxin-like PCBs specifically suppress hepatic PEPCK expression via the aryl hydrocarbon receptor. PLoS One *7*, e37103.